TECHNICAL REPORT BRL-TR-3334

BRL

ABSORPTION SPECTROSCOPY THROUGH THE DARK ZONE OF SOLID PROPELLANT FLAMES

JOHN A. VANDERHOFF
M. WARFIELD TEAGUE
ANTHONY J. KOTLAR

APRIL 1992

U.S. ARMY LABORATORY COMMAND

BALLISTIC RESEARCH LABORATORY
ABERDEEN PROVING GROUND, MARYLAND

NOTICES

Destroy this report when it is no longer needed. DO NOT return it to the originator.

Additional copies of this report may be obtained from the National Technical Information Service, U.S. Department of Commerce, 5285 Port Royal Road, Springfield, VA 22161.

The findings of this report are not to be construed as an official Department of the Army position, unless so designated by other authorized documents.

The use of trade names or manufacturers' names in this report does not constitute indorsement of any commercial product.

REPORT DOCUMENTATION PAGE

Form Approved
OMB No. 0704-0188

1. AGENCY USE ONLY (Leave blank)	2. REPORT DATE	3. REPORT TYPE AND DATES COVERED
	April 1992	Final, October 1990–October 1991

4. TITLE AND SUBTITLE

Absorption Spectroscopy Through the Dark Zone of Solid Propellant Flames

5. FUNDING NUMBERS

1L161102AH43

6. AUTHOR(S)

John A. Vanderhoff, M. Warfield Teague*, and Anthony J. Kotlar

7. PERFORMING ORGANIZATION NAME(S) AND ADDRESS(ES)

8. PERFORMING ORGANIZATION REPORT NUMBER

BRL-TR-3334

9. SPONSORING/MONITORING AGENCY NAME(S) AND ADDRESS(ES)

U.S. Army Ballistic Research Laboratory
ATTN: SLCBR-DD-T
Aberdeen Proving Ground, MD 21005-5066

10. SPONSORING/MONITORING AGENCY REPORT NUMBER

11. SUPPLEMENTARY NOTES

This work made possible by funding from the Army Productivity Capital Investment Program.
* Laboratory Research Cooperative Associate

12a. DISTRIBUTION/AVAILABILITY STATEMENT

Approved for public release; distribution is unlimited.

12b. DISTRIBUTION CODE

13. ABSTRACT *(Maximum 200 words)*

A windowed strand burner with a propellant feed mechanism has been used to characterize the steady-state combustion of solid propellants over a pressure environment of 0.1–2.0 MPa nitrogen. Under conditions where a line of sight measurement is meaningful, temperatures and absolute concentrations can be extracted from optical absorption spectra. An arc lamp light source and spectrometer-intensified photodiode array detector systems provided the means to acquire absorption spectra for NO through the dark zone burning solid propellants. Additionally, OH absorption spectra were obtained in the luminous flame region. A least-squares fitting program applied to these absorption spectra resulted in a determination of temperature profiles and absolute NO concentrations for JA-2, M-9, and HMX2 solid propellants over a pressure range of 0.3–2.0 MPa. Measured dark zone temperatures ranged from about 1,300 K to 1,600 K and NO concentrations varied from about 15 to 30 mole percent depending upon the propellant type and pressure. Where possible these values are compared with literature data. Temperatures in the luminous flame computed from OH absorption spectra reached values in agreement with adiabatic flame temperatures. Video records of each propellant burn allowed a determination of the propellant burn rate and length of the dark zone as a function of pressure.

14. SUBJECT TERMS	15. NUMBER OF PAGES
absorption; solid propellant; temperature; concentration; dark zone; spectroscopy; nitric oxide	51
	16. PRICE CODE

17. SECURITY CLASSIFICATION OF REPORT	18. SECURITY CLASSIFICATION OF THIS PAGE	19. SECURITY CLASSIFICATION OF ABSTRACT	20. LIMITATION OF ABSTRACT
UNCLASSIFIED	UNCLASSIFIED	UNCLASSIFIED	SAR

INTENTIONALLY LEFT BLANK.

TABLE OF CONTENTS

		Page
	LIST OF FIGURES	v
	LIST OF TABLES	vi
1.	INTRODUCTION	1
2.	EXPERIMENTAL	2
3.	DATA ANALYSIS	6
4.	RESULTS	8
4.1	Burn Rates and Dark Zone Lengths	8
4.2	Absorption - JA-2 Propellant	8
4.3	Absorption - M9 Propellant	21
4.4	Absorption - HMX2 Propellant	26
5.	SUMMARY	26
6.	REFERENCES	33
	DISTRIBUTION LIST	35

INTENTIONALLY LEFT BLANK.

LIST OF FIGURES

Figure		Page
1.	A Cross Section of the Windowed Strand Burner Chamber	3
2.	A Top View of the Four Optical Paths (Video, Emission, and Two Absorption Paths) Used in Obtaining Combustion Diagnostic Data on Solid Propellant Flames	5
3.	The Burn Rate of JA-2 as a Function of Nitrogen Pressure	9
4.	The Burn Rate of M9 as a Function of Nitrogen Pressure	10
5.	The Burn Rate of HMX2 as a Function of Nitrogen Pressure	11
6.	The Distance From the JA-2 Propellant Burning Surface to the Luminous Flame (the Dark Zone) as a Function of Nitrogen Pressure	12
7.	The Dark Zone Length of M9 Propellant as a Function of Nitrogen Pressure	13
8.	The Dark Zone Length of HMX2 Propellant as a Function of Nitrogen	14
9.	Rotationally Resolved (0,1) $A^2\Sigma$ - $X^2\Pi$ Transitions in NO Taken in an Atmospheric Pressure CH_4 /N_20 Flame	15
10.	NO Absorption Spectrum Taken in the Dark Zone of JA-2 Burning in 0.68 MPa Nitrogen	16
11.	Rotationally Resolved OH Absorption Spectrum Taken in the Luminous Flame Region of JA-2 Burning in 1.6 MPa Nitrogen	17
12.	Absolute Concentrations for NO (∘) and OH (•) as a Function of Distance From the JA-2 Propellant Surface Burning in 1.6 MPa Nitrogen	19
13.	Temperature Profile for JA-2 Propellant Burning in 1.6 MPa Nitrogen	20
14.	Dark Zone NO Concentration vs. Pressure for JA-2 Propellant Burning in Nitrogen	22
15.	Dark Zone Temperatures as a Function of Pressure for JA-2 Propellant Burning in Nitrogen	23
16.	NO and OH Concentrations Through the Dark Zone of M9 Propellant Burning in 1.7 MPa Nitrogen	24
17.	Temperature Profile Through the Dark Zone of M9 Propellant Burning in 1.7 MPa Nitrogen	25

18. NO Concentration in the Dark Zone of M9 Propellant Obtained as a Function of Pressure 27

19. Dark Zone Temperature as a Function of Pressure for M9 Propellant 28

20. NO Concentration as a Function of Distance From the Propellant Surface for HMX2 Burning in 1.9 MPa Nitrogen 29

21. Temperature as a Function of Distance From the Propellant Surface for HMX2 Burning in 1.9 MPa Nitrogen 30

LIST OF TABLES

Table — Page

1. Propellant Characteristics 2

2. Comparison of Temperatures and NO Concentrations in the Dark Zone of Various Propellants 31

1. INTRODUCTION

Solid propellants burning at moderate pressures exhibit distinctly different visual characteristics depending on their composition. Many propellants sustain two flames in the gas phase which are separated by a dark zone at low pressure. The length of this zone increases with decreasing pressure and for sufficiently low pressure the luminous flame may not be observed. At high pressures these flames merge. Most common Army gun propellants—single base (nitrocellulose), double base (nitrocellulose-nitroglycerin) and low vulnerability nitramine—exhibit a nonluminous zone (dark zone) which arises from the slow conversion of NO to N_2. The production of energetic species from incomplete combustion at these moderate pressures could play a role in delayed ignitions which are found to occur in some gun firings and, thus, it is of interest to study the fate of the gas phase NO through the combustion zones. Moreover, several papers have been written on a detailed chemistry model for the dark zone of propellants and these models require experimental data to test their validity. Here also, experimental NO diagnostic data through the gas phase combustion zones can be helpful since there is a scarcity of this type of propellant data available in the published literature.

Sotter (1965) was the first to model the dark zone of a double-base propellant using 20 chemical reactions. Fifer et al. (1990) have recently modelled the dark zone of a double-base and a composite propellant using much more extensive chemistry, and Bizot and Beckstead (1988) have constructed a double-base propellant model which includes both the condensed and gas phases. Experimental data for model comparison is quite limited. While there is often measurements which report propellant burn rate and dark zone length as a function of pressure, very few experiments also give the temperature and species concentration profiles. Data of Heller and Gordon (1955), Kubota (1982), and Lengelle et al. (1984) are the only known sources that report such complete data sets.

These published measurements use microthermocouples for the temperature measurement and gas probe sampling for the determination of the gas composition. The compositions are determined from either infrared analysis or mass spectroscopy. Since H_2O is condensable in the probe, it's concentration is determined by matching the elemental composition with that of the initial propellant. The temperatures and concentrations that we report here come from an optical absorption technique which has several advantages. No physical probe is required for sampling and the data are obtained in situ. For completeness, burn rate and dark zone length measurements as a function of pressure as well as temperatures and NO concentrations for three different propellants are reported. The propellant

ingredients, flame temperatures, and heats of explosion are summarized in Table 1. The adiabatic flame temperatures are calculated with the NASA-Lewis Code (Svehla and McBride 1973) for constant pressure conditions and the heats of explosion are measured quantities that are included in the propellant description sheets.

Table 1. Propellant Characteristics

Propellant	Main Ingredients (Wt %)	Equil. Flame Temperature (K)	Heat of Explosion (cal/g)
JA-2	58% Nitrocellulose* 16% Nitroglycerin 25% DEGDN	2,791 @ 1.5 MPa	1,120
M9	58% Nitrocellulose** 40% Nitroglycerin 1.6% KNO_3	3,019 @ 1.5 MPa	1,308
HMX2	80% HMX 20% PE Binder	2,045 @ 1.5 MPa	780

HMX - cyclotetramethylenetetranitramine, PE - polyester binder based on polydiethylene glycol adipate, DEGDN - diethyleneglycoldinitrate, * - 13.04% N, ** - 13.29% N

2. EXPERIMENTAL

Vibrationally and rotationally resolved absorption spectroscopy of NO and OH has been experimentally studied in three different solid propellant flames as well as in a steady-state CH_4/N_2O flame which was used for optimization purposes. The burner and windowed combustion chamber used for this work has been described previously (Vanderhoff 1988; Vanderhoff 1991) and, thus, only a brief description will be provided here with an emphasis on new features. A cross-sectional drawing of the stainless steel, windowed chamber is shown on Figure 1. This chamber provides a constant pressure flowing environment for burning solid propellants. The flow rate of nitrogen gas channeled around the propellant to form a shroud is maintained at about four times the propellant gasification rate with a critical orifice. The pressure history has been monitored with an MKS pressure transducer. In the present configuration, the chamber is capable of a pressure range from 0.1 to 2.0 MPa. A wire which is rapidly heated forms the ignition source for the cylindrical propellant sample. Once ignited, the propellant burns

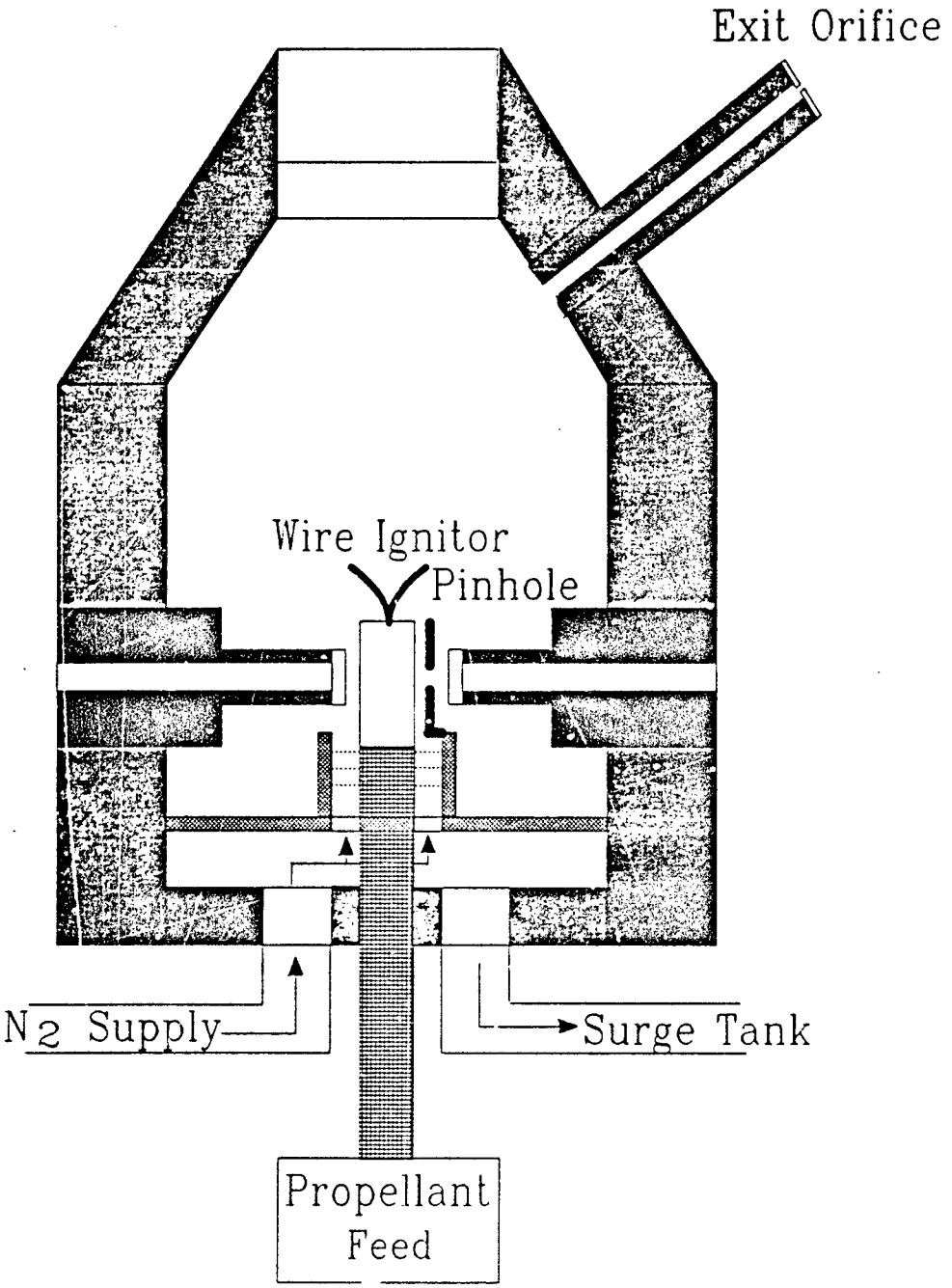

Note: The window extensions added to minimize the absorption path are highlighted in black.

Figure 1. A Cross Section of the Windowed Strand Burner Chamber (Not to Scale).

downward in cigarette fashion. After burning a distance of about 0.5 cm, the light apertured by the pinhole is able to transit across the propellant surface to the detector. Figure 2 illustrates this condition which is the beginning of actual absorption data and represents zero distance from the propellant surface. The transmitted light is continuously sampled for many time segments (0.02–0.1 s) for the duration of the propellant burn (5–15 s). If the absorption signals are strong, the propellant sample is held fixed in place; however, for weak absorption signals, the data acquisition time is lengthened by pushing the propellant upward at a rate near the burn rate of the propellant. This movement of the propellant is accomplished by a unidirectional-constant-speed-stepper-motor-table which is coupled to the propellant sample by a plastic shaft swage fitted to the pressure vessel. This swage fitting is tightened enough to hold pressure, but allowing linear motion without excessive force. One of the new features of the chamber is the minimization of the absorption path length inside the chamber housing. This has been accomplished by mounting quartz windows on the ends of extenders, as shown in Figure 1. The total path length is only about double the propellant sample diameter (0.65 cm) and should include only the emerging propellant gases and shroud gas.

The top view of the optical paths for emission, absorption, and video is shown in Figure 2. A video record is taken for each propellant burn experiment; burn rates, dark zone lengths, and the one-dimensionality of the burn can be extracted from these S-VHS movies. Much of the quantitative data are determined from absorption spectra of diatomic combustion intermediates. The excitation light source for the absorption measurements is a 500-W xenon arc lamp. We have recently added a second absorption detection system so that two or more species can be monitored simultaneously. A broadband beamsplitter divides, about equally, the apertured light that has passed through the combustion region of the burning propellant. These signals are focussed into two 0.32-m spectrometers which disperse the light across the active region of intensified photodiode array detectors. Depending upon the spectrometer grating and entrance slit, the spectral resolution varied from 0.03 to 0.3 nm giving a wavelength capture range of 6–24 nm for the intensified photodiode arrays. The spatial resolution in the vertical (burning direction) was set by the pinhole aperture in close proximity to the propellant sample; two sizes—0.1 and 0.2 mm—have been used. In the absorption experiments, the accompanying emission signal is made negligible by placing a sufficiently small aperture between the propellant sample and the detectors. Various filters have also been used in the absorption experiments to either minimize stray light or to reject first-order light when operating the spectrometer in second order.

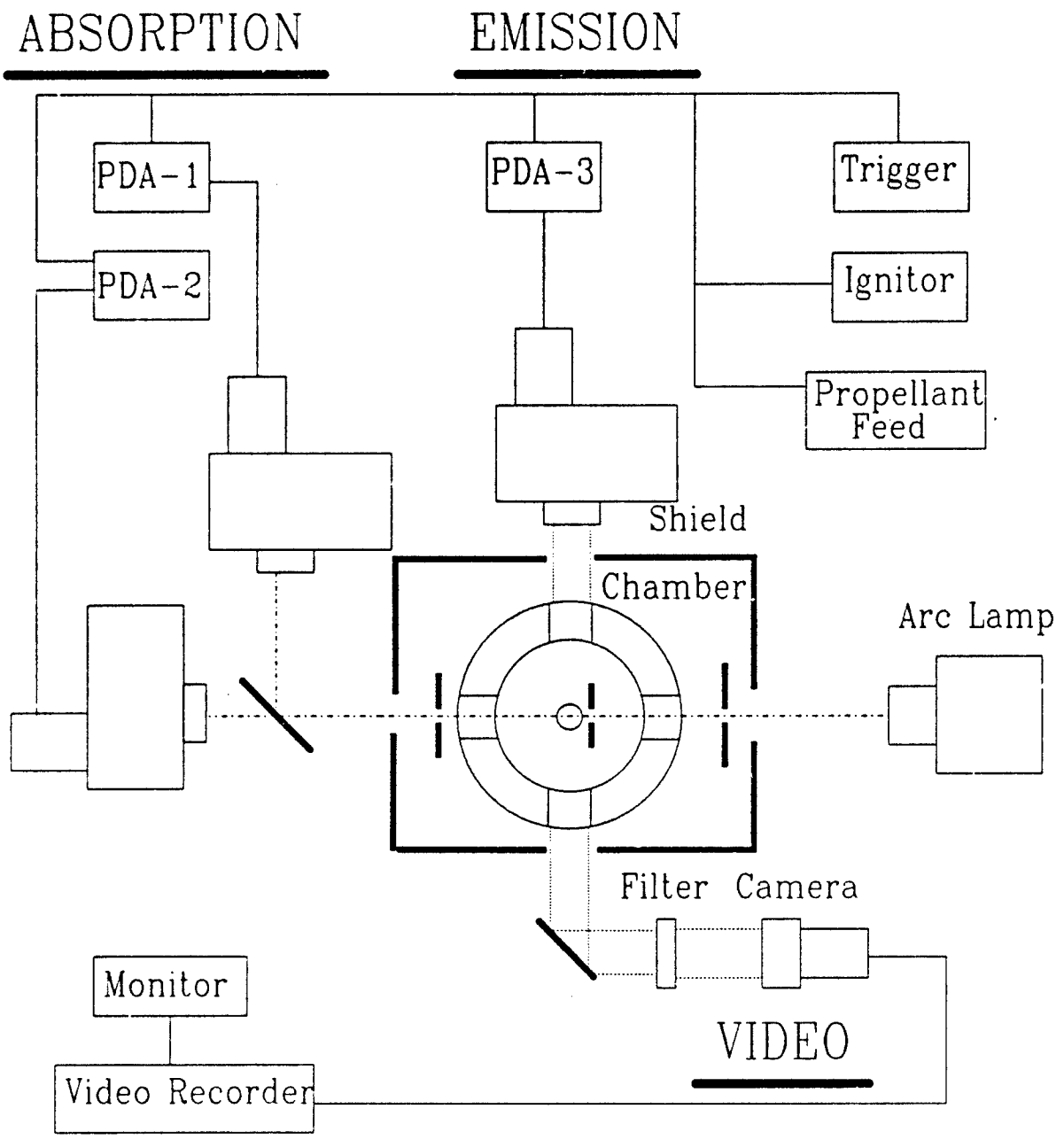

Figure 2. A Top View of the Four Optical Paths (Video, Emission, and Two Absorption Paths) Used in Obtaining Combustion Diagnostic Data on Solid Propellant Flames.

Propellant samples were approximately cylindrical with a nominal diameter of 0.65 cm and a length of 2 cm. When it was necessary to use the propellant feed mechanism the length was increased to 4 cm. JA-2 and M9 propellant samples made in a cylindrical shape and the HMX2 samples were originally rectangular in shape. However, the rectangular shape produced a nonplanar burn; hence, they were shaved such that a cylindrical shape was approximated. Unfortunately, this shaving caused the propellant sample to burn down the sides as well as from the top. To eliminate this behavior, the HMX2 samples were coated with a thin layer of fingernail polish. The burner head supporting the steady-state CH_4/N_2O flame was small. It was composed of several dozen small holes with an overall diameter of 0.4 cm. For optimization and calibration purposes the burner was positioned at the place normally occupied by the propellant sample.

3. DATA ANALYSIS

The purpose of the diagnostic technique implemented here is to extract temperature and concentration from absorption spectra by a least-squares fitting procedure using an equation of the form

$$I_w = \int S(w, w_o) I(w) dw \qquad (1)$$

where I_w, the integrated light transmitted, is a function of w_o, the index wavelength of the photodiode array. $S(w, w_o)$ is an instrument function appropriate for the spectral resolution of the detection system and I(w) is the transmitted intensity of a group of lines for a given species. A more complete description of the absorption equations and fitting technique can be found elsewhere (Vanderhoff 1991; Vanderhoff and Kotlar 1990b; Lucht, Peterson, and Laurendeau 1978). During the investigations of absorption in propellant combustion gases over the spectral region of 200–400 nm, substantial attenuation of the transmitted light beam was observed. This attenuation (absorption) was broadband (i.e., not a strong function of wavelength). For cases where this attenuation (assumed to be a background) is large, proper handling of the background becomes important. In simple terms, an absorption experiment is governed by an expression for the transmitted light intensity (I) which can be written as

$$I = I_o \exp[-k_w l] + B_o \qquad (2)$$

where I_o is the incident light intensity from the arc lamp, k_w is the absorption coefficient the molecule of interest, l is the path length for absorption, and B_o is a baseline correction factor. This correction factor

is commonly used to adjust the data for small drifts in the experimental system such as output changes in the arc lamp and/or gain changes in the detection system. In the present experimental arrangement these adjustments are not necessary since the entire wavelength range of interest for the absorption spectra is gathered simultaneously with the intensified photodiode array. However, it is essential to make a baseline correction for the large broadband attenuation observed. Sources for this attenuation are scattering from particulates and/or broadband absorption of light from large molecules. The attenuation occurs as the light transits the combustion zone and, thus, is path length-dependent so the transmitted intensity can be expressed as

$$I = I_o \exp[-k_w - b_w]l \tag{3}$$

where the attenuation correction is included in the exponential. Moreover, since the attenuation is not a strong function of wavelength, Equation 3 is approximated as

$$I = I_o \exp[-b_w l]\exp[-k_w l] = I_o B(w)\exp[-k_w l]. \tag{4}$$

The baseline correction is now represented as a multiplicative factor rather than an additive one. It is this form that is used in the reduction of the data presented in this report. The observed shape of the experimental baseline is used to determine the appropriate form of B(w). For all the data analyzed using Equation 4, B(w) is taken to be linear (i.e., $B(w) = B_1 w + B_2$).

Equation 1 is fitted with a multivariate nonlinear least-squares technique to determine the optimum values of temperature and species concentration for a given absorption spectrum. For high-resolution absorption spectra (OH spectra), the fit with respect to wavelength appeared shifted in a nonlinear fashion. Further investigation into this area revealed that, when a spectrometer is used with an array detector, the relationship between wavelength and photodiode position is not linear. Hence, the least-squares fitting also included an algorithm for wavelength nonlinearity which is described elsewhere (Vanderhoff and Kotlar 1990a; Vanderhoff, Kotlar, and Teague 1990).

The absorption transitions probed for OH and NO are in the $A^2\Sigma$ - $X^2\Pi$ electronic system. For OH, 153 rotational transitions over the wavelength range from 306 to 310 nm were included in the absorption calculation and fit. Two main vibrational bands, the (0,1) and the (0,2), were probed for absorption for the NO case. The dark zone of these propellants contained enough NO to produce 100% absorption in

the (0,0) band and, thus, it was of no use. Even though the (1,3) band for NO showed no detectible absorption (Figure 10), it was included in the absorption calculation. Inclusion of these three vibrational bands made it necessary to calculate a total of 2,079 rotational transitions. Although it is possible to operate the detection system with sufficient resolution to rotationally resolve the NO transitions, it was felt that (for the propellant case) there was not a sufficient portion of the spectra for keeping track of the background contribution. One rotationally resolved NO spectrum for the steady-state flame is shown in the results section (Figure 9) to indicate how well the calculation can agree with the data for the position and intensity of the rotational absorption transitions. The values for the molecule-specific information necessary to extract temperature and concentrations from absorption data have been given previously (Vanderhoff, Kotlar, and Teague 1990; Huber and Herzberg 1979).

4. RESULTS

4.1 Burn Rates and Dark Zone Lengths. Although not a primary goal of this report, the burn rate and dark zone length data for the three propellants studied are essential pieces of information for performing modelling of these combustion processes. Burn rates and dark zone lengths as a function of pressure for JA-2, M9, and HMX2 are shown in Figures 3–8, respectively.

4.2 Absorption - JA-2 Propellant. As a check on the molecular parameters for NO, a high-resolution absorption spectrum for NO was obtained in an atmospheric CH_4/N_2O flame. This spectrum and corresponding least-squares fit are illustrated in Figure 9. Using literature values for the NO molecular parameters, experimentally determined values for the instrument response functions, least-squares fitted values for the temperature, NO concentration, instrumental wavelength nonlinearity, and baseline, the band origins and rotationally resolved transitions are fitted extremely well over the entire (0,1) vibrational band envelope. The least-squares fit to the data is shown as a solid line and represents a temperature of 1,868 K and an NO mole fraction of 0.05. An acquisition time of about 1.0 min was required to obtain the data displayed in Figure 9. A combination of larger pressures and NO concentrations made it possible to gather NO absorption spectra much faster (≈ 0.1 s) when probing the dark zone of the propellants studied here. Examples of the types of NO and OH absorption spectra obtained and used for extracting temperatures and absolute NO and OH concentrations are shown in Figures 10 and 11, respectively. The NO spectrum was obtained in the dark zone of JA-2 propellant burning in 0.68 MPa nitrogen. Both the (0,1) and (0,2) vibrational transitions of the $A^2\Sigma$ - $X^2\Pi$ system of NO are clearly observed. The (1,3) vibrational transition also occurs over this wavelength range, but the absorption is too small to be observed

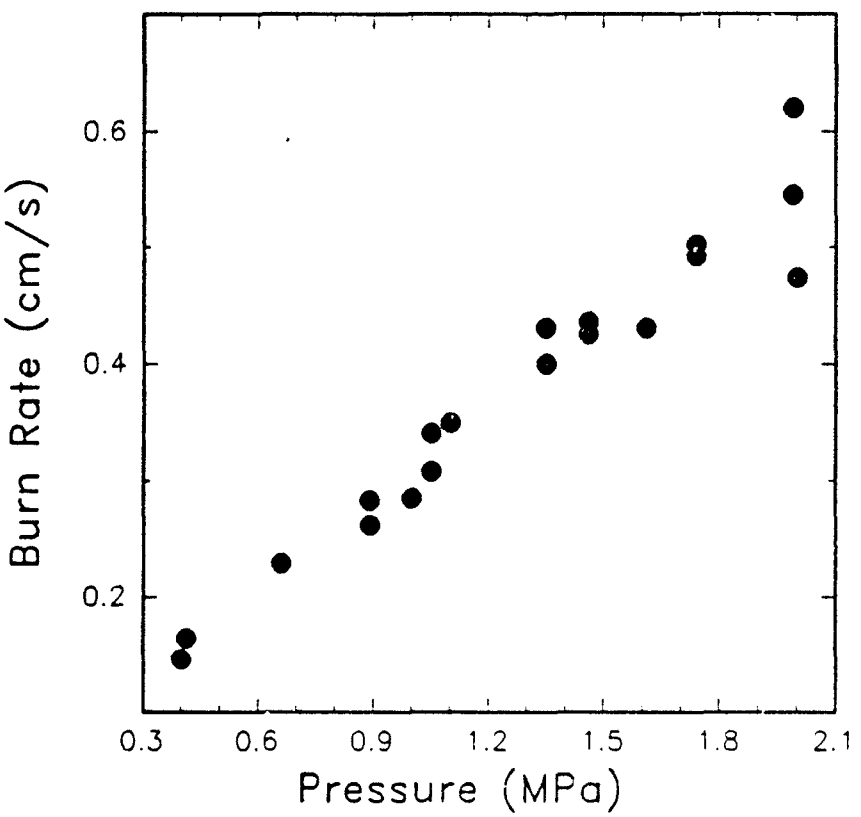

Figure 3. The Burn Rate of JA-2 as a Function of Nitrogen Pressure.

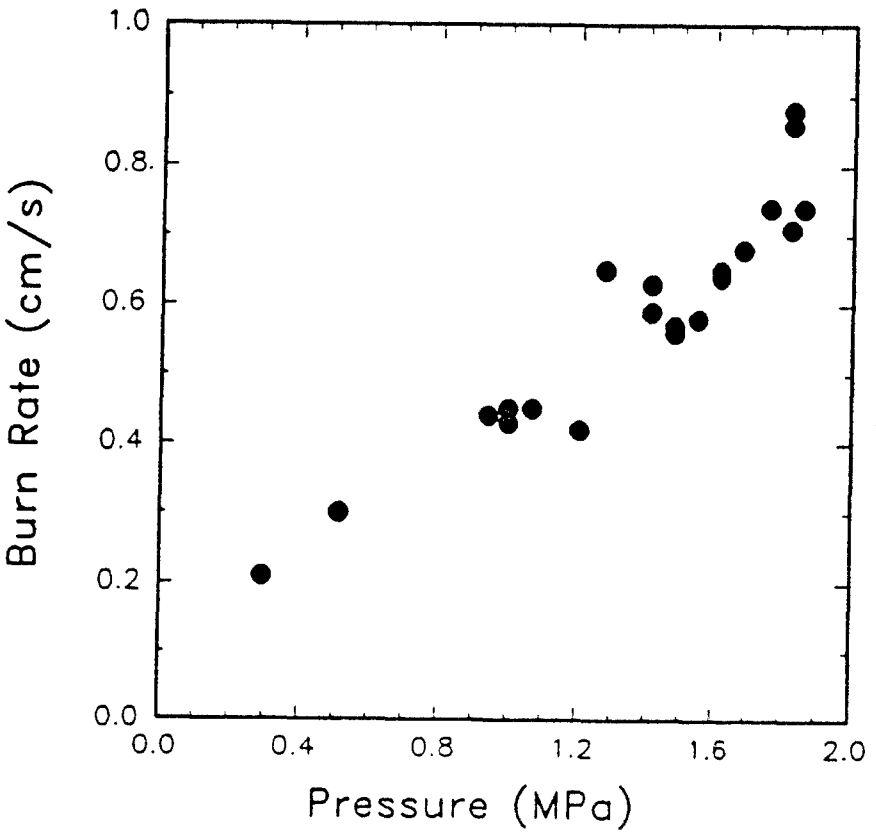

Figure 4. The Burn Rate of M9 as a Function of Nitrogen Pressure.

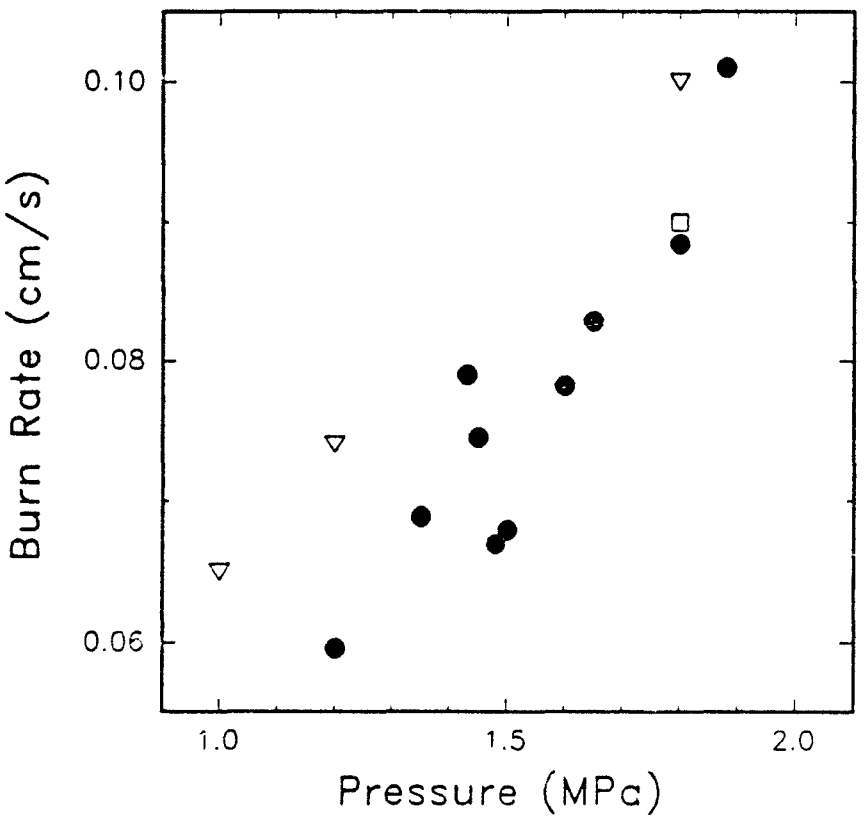

Note: Our data (•), the data of Kubota (1982) (▽), and the data of Edwards (1988) (□).

Figure 5. The Burn Rate of HMX2 as a Function of Nitrogen Pressure.

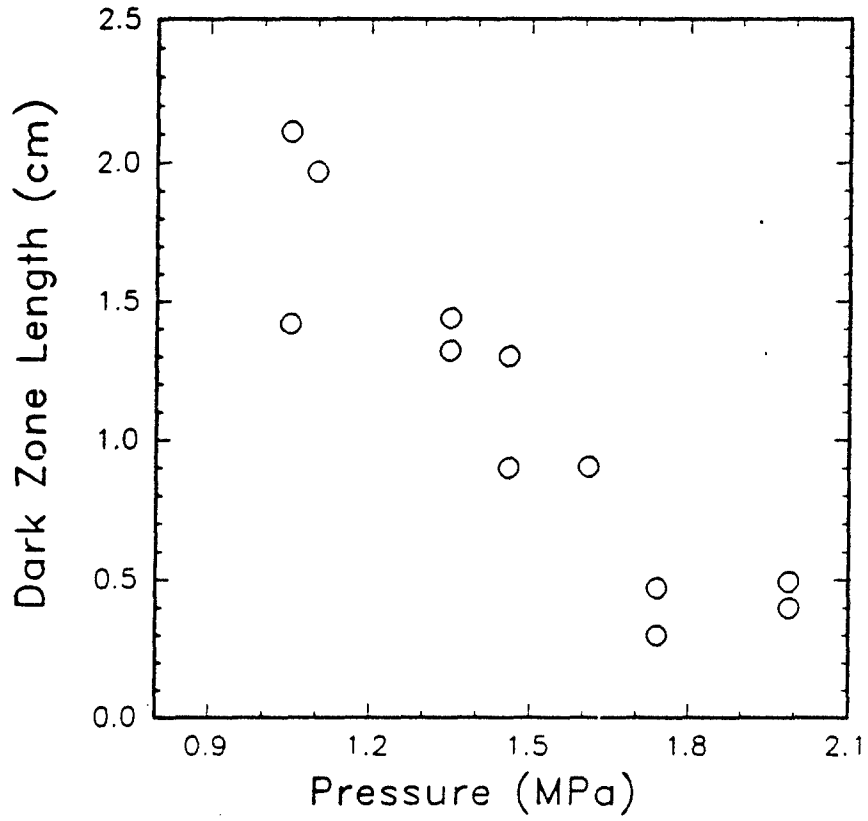

Figure 6. The Distance From the JA-2 Propellant Burning Surface to the Luminous Flame (the Dark Zone) as a Function of Nitrogen Pressure.

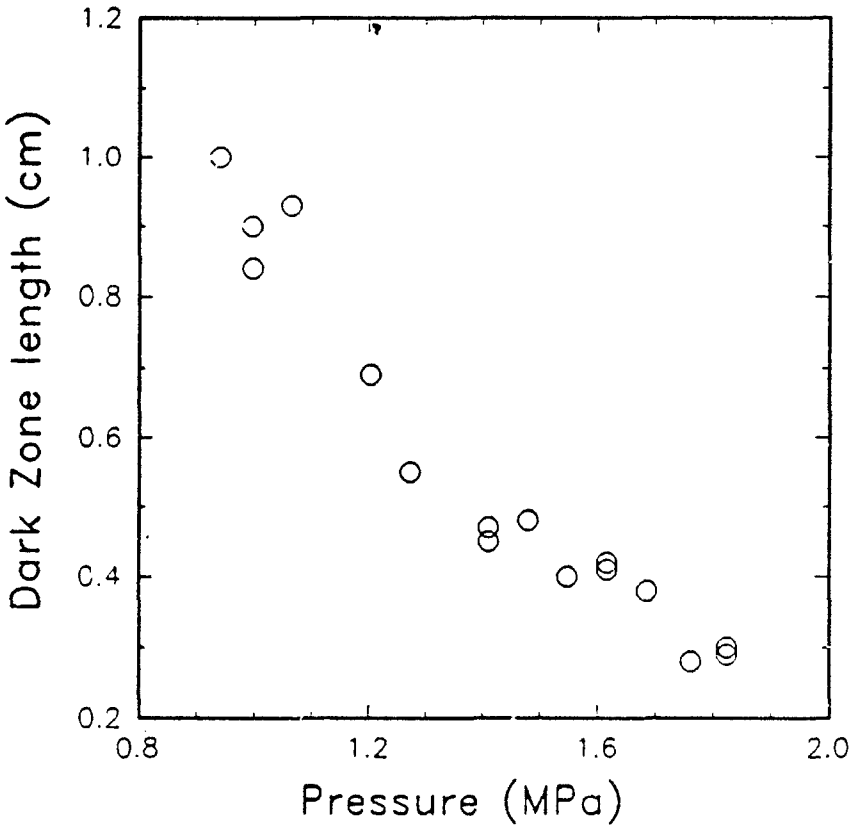

Figure 7. The Dark Zone Length of M9 Propellant as a Function of Nitrogen Pressure.

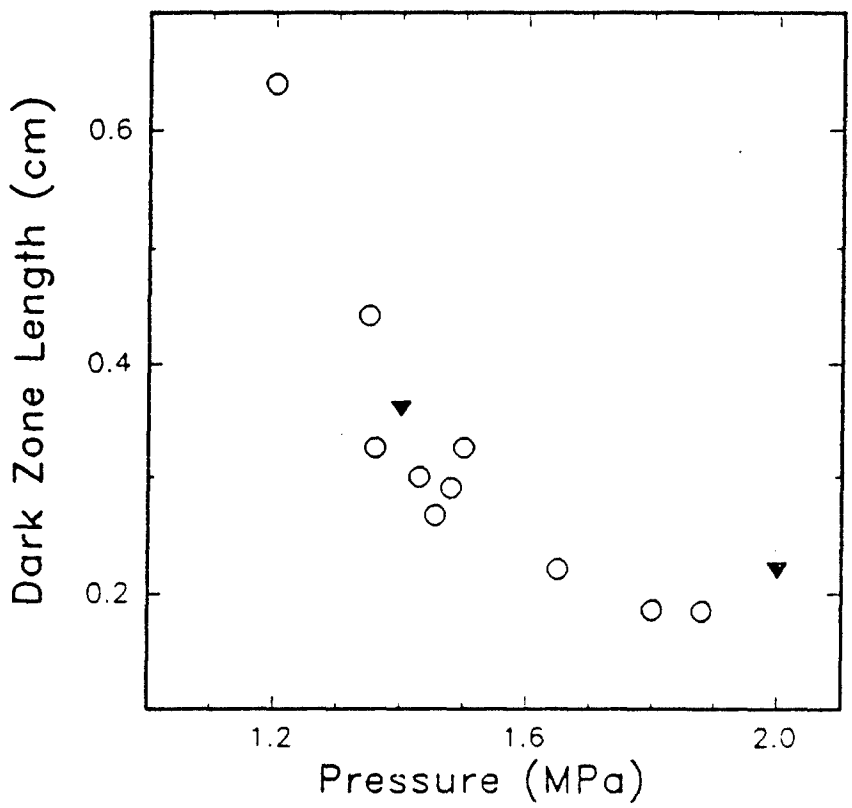

Note: Our data (○) and the data of Kubota (1982) (▼).

Figure 8. The Dark Zone Length of HMX2 Propellant as a Function of Nitrogen.

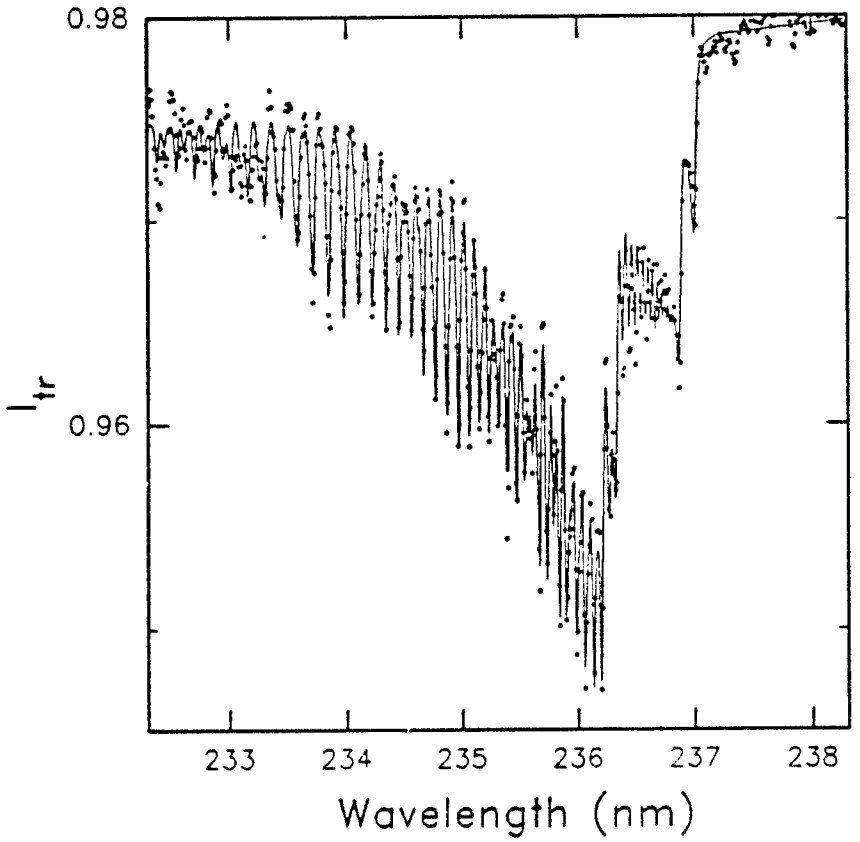

Figure 9. Rotationally Resolved (0,1) $A^2\Sigma$ - $X^2\Pi$ Transitions in NO Taken in an Atmospheric Pressure CH_4/N_2O Flame.

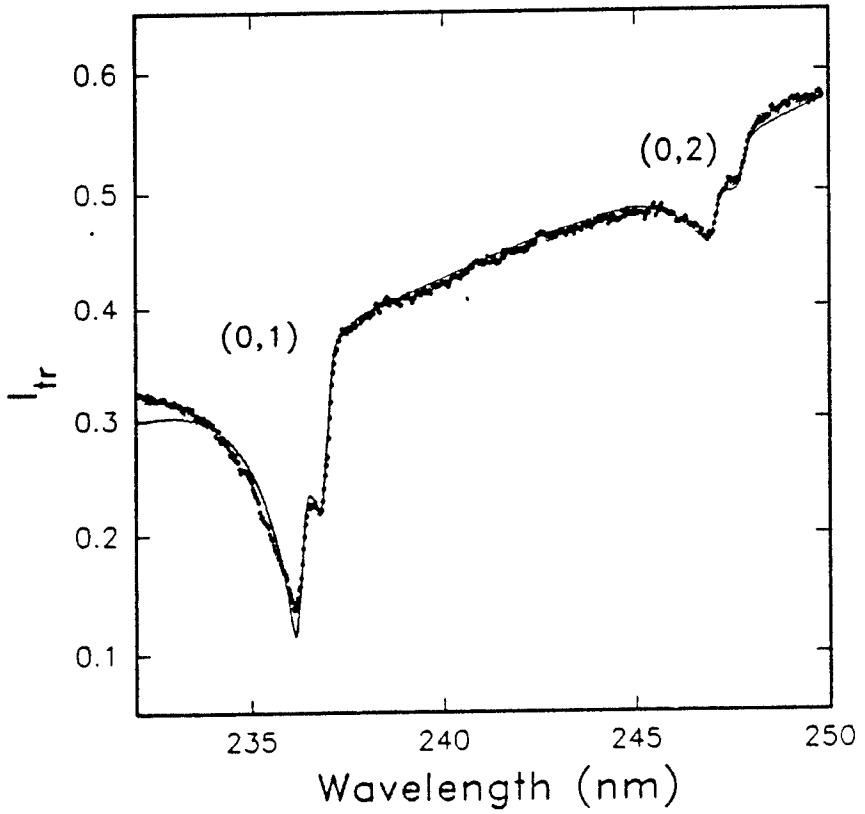

The solid points are the data and the solid line is a least squares fit to the data..

Figure 10. NO Absorption Spectrum Taken in the Dark Zone of JA-2 Burning in 0.68 MPa Nitrogen.

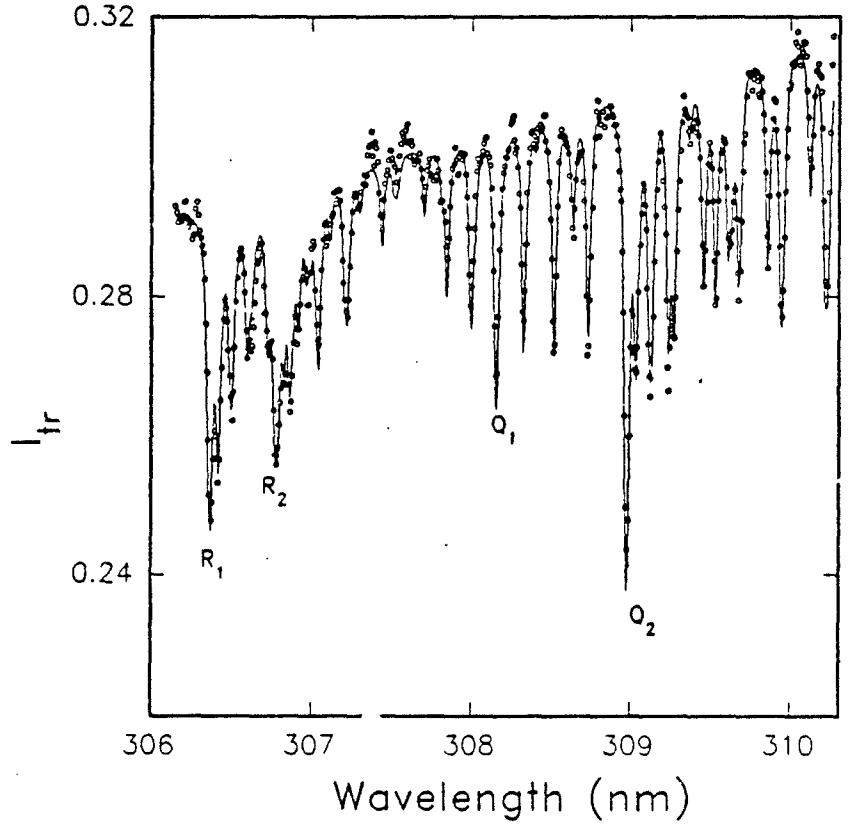

Figure 11. Rotationally Resolved OH Absorption Spectrum Taken in the Luminous Flame Region of JA-2 Burning in 1.6 MPa Nitrogen.

in Figure 10. Total absorption of the light source occurred for the (0,0) transition and, thus, was not usable. The resolution of the NO detection system (0.06 nm) was set low enough to include two vibrational transitions and, thus, the rotational structure is not resolved. Nonetheless, in the least-squares fitting calculation, a total of 2,073 rotational transitions were used to calculate the vibrational band envelopes. The least-squares fit to the data of Figure 10 results in best values for temperature and NO concentration which are 1,350 K and 0.25 mole fraction. The absorption spectrum for OH (shown on Figure 11) was obtained in the luminous flame region of JA-2 burning in 1.6 MPa nitrogen. Here the OH detection system was set to a spectral resolution of 0.03 nm—twice that for NO. This is sufficient to resolve the rotational transitions within the (0,0) $A^2\Sigma$ - $X^2\Pi$ system, as can be observed. R_1, R_2, and Q_2 are rotational branch heads, but many of the transitions in the Q_1 region are isolated lines. Over this wavelength range, 128 rotational transitions have been included in fitting the OH spectra. The least-squares fit to the spectrum of Figure 11 results in a temperature of 2,690 K and OH mole fraction of 0.002. Computer fitting of the NO and OH absorption spectra was accomplished on a 386/33 PC. The time to complete a fit depends on the number of transitions included and was, in general, less than 10 min for a typical good fit.

Many absorption spectra (around 30) like those on Figures 10 and 11 are accumulated during the time for one propellant burn. By measuring the burn rate of the propellant, these spectra can be assigned to distances above the propellant surface. Concentrations and temperatures as a function of distance from the propellant surface are thus determined and illustrated in Figures 12 and 13, respectively. As can be seen from Figure 12, large quantities of NO are present close to the propellant surface and persist over a distance of about 0.8 cm at this pressure. At about 0.8 cm from the propellant surface, the NO concentration drops rapidly with distance and the luminous flame is formed. A large energy release in this region causes an increase in temperature which produces amounts of OH sufficient for obtaining good quality absorption spectra. These spectra provide the data from which luminous flame temperatures can be determined. The luminous flame temperatures shown as solid points on Figure 13 attain values in agreement with the adiabatic flame temperature (2,792 K and shown as a dashed line on Figure 13) calculated with the NASA-Lewis (Svehia and McBride 1973) code for constant pressure conditions. The OH concentration computed using the adiabatic flame temperature is 0.0047. Maximum OH concentrations determined from absorption spectra and displayed as the solid points on Figure 12 are about a factor of 2 lower than the equilibrium value. There are several reasons why this difference should not be surprising. First, these measurements are made at distances from the surface larger than the propellant diameter and the one-dimensional geometry (the path length for absorption) may not obtain at these

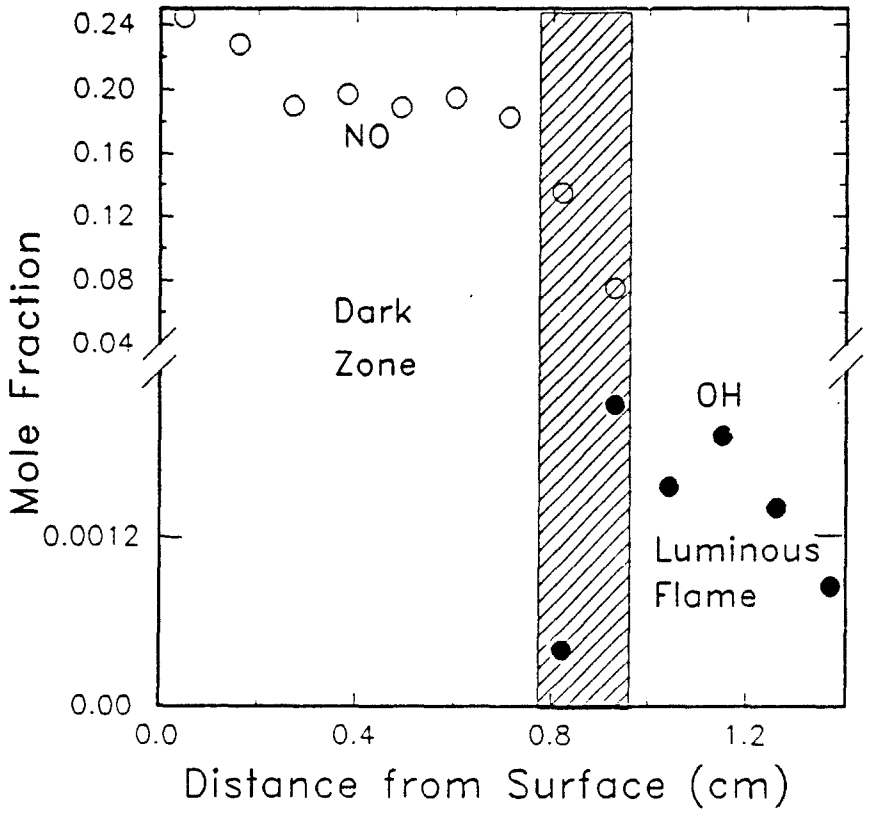

Note: The hashed region depicts the variation in the position of the luminous flame front.

Figure 12. Absolute Concentrations for NO (○) and OH (●) as a Function of Distance From the JA-2 Propellant Surface Burning in 1.6 MPa Nitrogen.

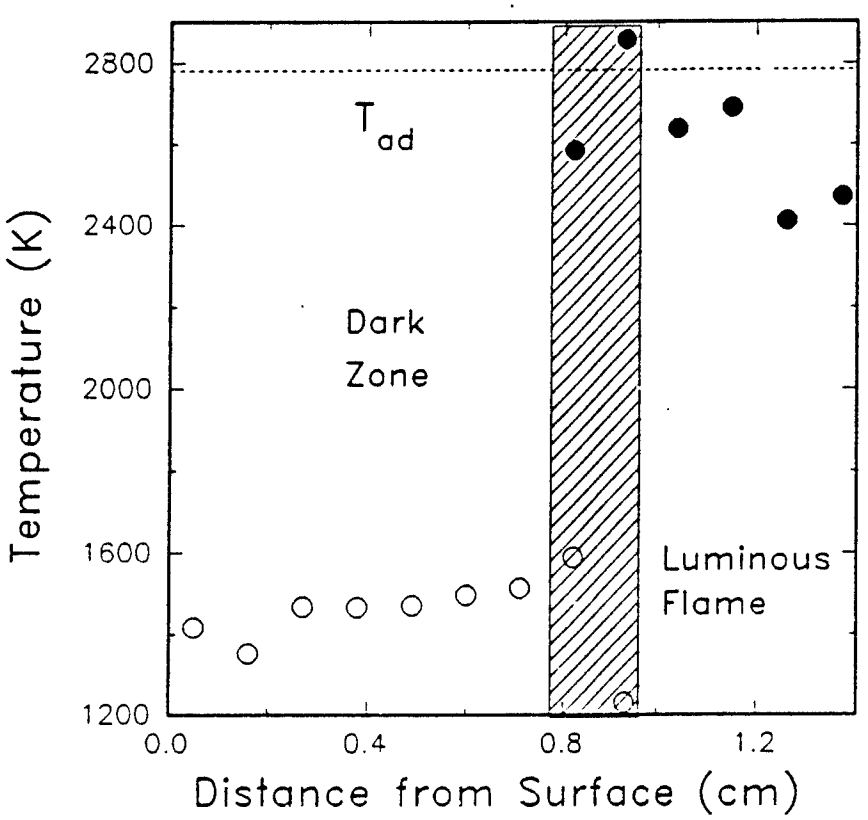

Note: Dark zone temperatures (∘) are from NO absorption spectra and luminous flame temperatures (•) are from OH absorption spectra.

Figure 13. Temperature Profile for JA-2 Propellant Burning in 1.6 MPa Nitrogen.

distances. Second, the OH concentration is highly dependent on temperature. If the flame temperature is lowered by about 3.5% (100 K), the equilibrium OH concentration is lowered by a factor of 2.

Video records of the propellant burn reveal that the luminous flame front does not remain at a fixed distance from the propellant surface and the range over which the flame front occurs is approximated by the hashed region. The scatter in the flame front position and in the data obtained for greater distances from the propellant surface are probably due in part to the finite geometry of the propellant sample. Nonetheless, the data of most interest, the dark zone region, is closer to the propellant surface. Here the NO mole fraction starts at about 0.24 and slowly decreases to a value of about 0.19 at a distance of 0.8 cm from the surface. In the luminous flame front region the NO concentration drops substantially. From Figure 7 it is also observed that the temperature close to the propellant surface is about 1,400 K and increases slightly to about 1,500 K at 0.8 cm from the propellant surface. Within experimental uncertainty it is possible to interpret Figures 12 and 13 as indicating constant temperature and NO concentration, however, the trends are consistent with propellant models (Sotter 1965; Fifer et al. 1990; Bizot and Beckstead 1988).

The pressure dependence of temperature and NO concentration in the dark zone is shown on Figures 14 and 15, respectively. The data, shown thus far, plotted as a function of distance or wavelength represents one experiment or propellant burn, but the data plotted as a function of pressure represents as many propellant burns as there are data points. It can be observed (and is expected) that these data have more scatter. This scatter is more representative of the uncertainties associated with the temperature and NO concentration data reported in this paper.

Each value of NO concentration and temperature plotted in Figures 14 and 15 represents an average of four spectra taken as a function of position early in the dark zone. Again, within experimental uncertainty, it is possible to interpret Figures 14 and 15 as indicating that the dark zone temperature and NO concentration are constant. Nonetheless, the trends which indicate the dark zone temperature is slightly increasing with pressure and the NO concentration is slightly decreasing with pressure are consistent with previous double-base propellant data (Heller and Gordon 1955) and thermochemical equilibrium calculations (Svehla and McBride 1973).

4.3 Absorption - M9 Propellant. Analogous to Figures 12 and 13, NO and OH concentrations and temperatures through the dark zone of a double-base propellant (M9) burning in 1.7 MPa nitrogen are plotted in Figures 16 and 17, respectively. Here also the luminous flame front is unstable and its spatial

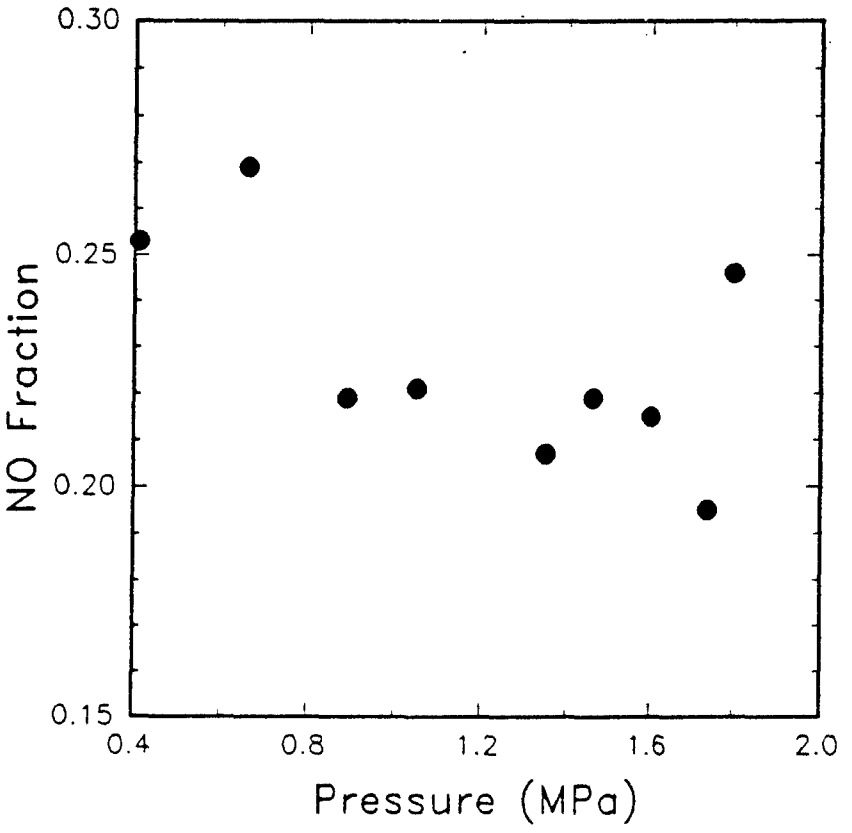

Figure 14. Dark Zone NO Concentration vs. Pressure for JA-2 Propellant Burning in Nitrogen.

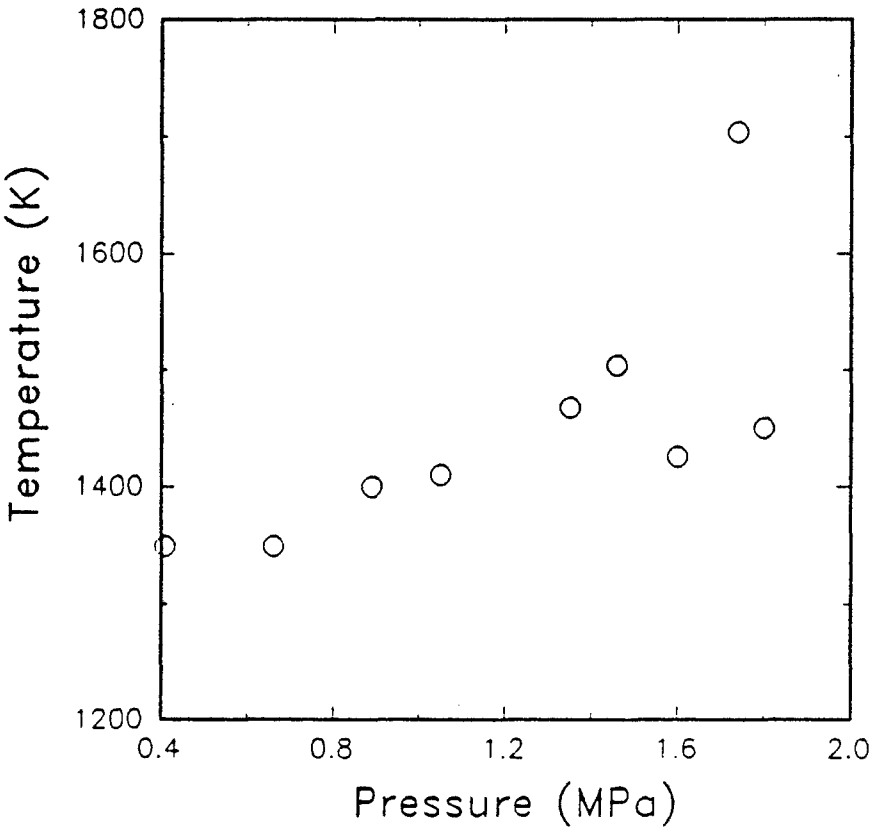

Figure 15. Dark Zone Temperatures as a Function of Pressure for JA-2 Propellant Burning in Nitrogen.

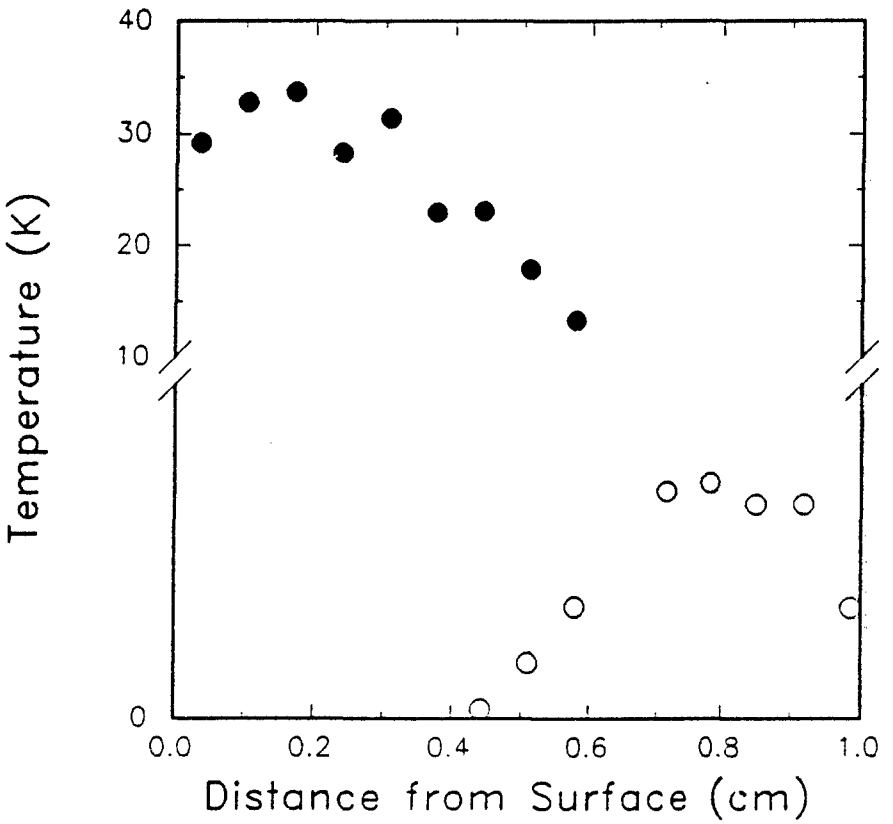

Note: The solid circles are NO concentration and the open circles are OH concentration.

Figure 16. NO and OH Concentrations Through the Dark Zone of M9 Propellant Burning in 1.7 MPa Nitrogen.

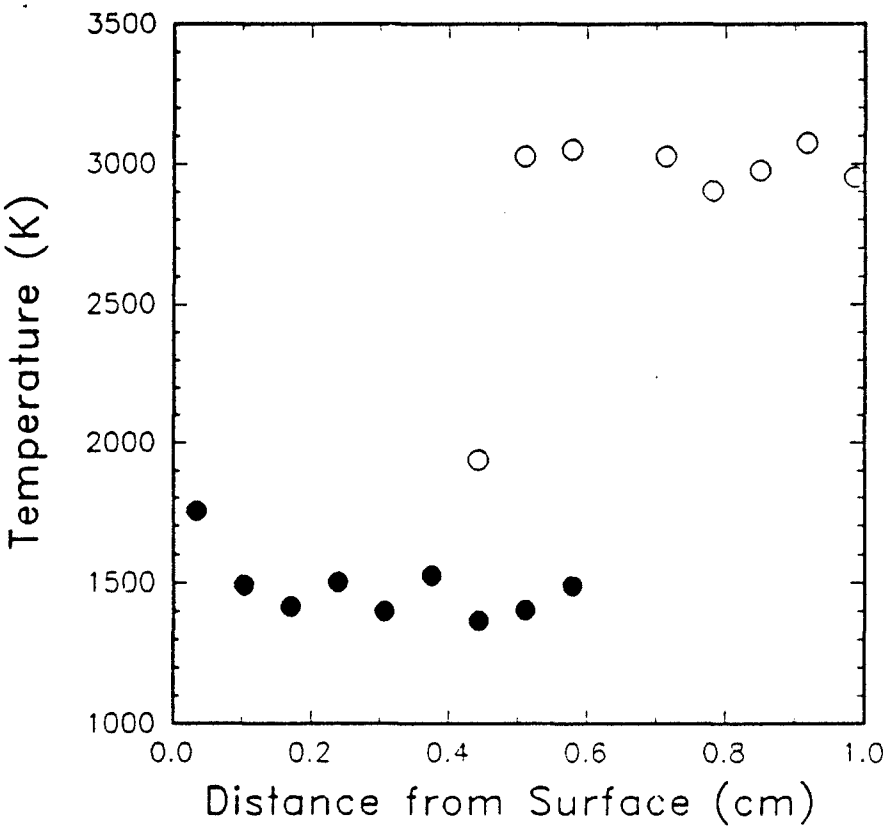

Note: The solid points are temperatures derived from NO absorption spectra and the open circles are temperatures from OH absorption spectra.

Figure 17. Temperature Profile Through the Dark Zone of M9 Propellant Burning in 1.7 MPa Nitrogen.

position varies over about a 0.2 cm extent, similar to what was observed for JA-2 and designated with a hashed area. The NO concentration stays about constant at a mole fraction of 0.3 out to a distance of 0.3 cm from the M9 propellant surface. At about 0.4 cm from the surface, the OH absorption becomes measurable and the OH concentration plateaus close to the thermochemical equilibrium value which is 0.018. The dark zone temperature is about constant at 1,450 K through the dark zone and then jumps to temperatures in agreement with the adiabatic flame temperature (3,020 K). In contrast, the pressure dependence of the NO concentration and dark zone temperature contains considerable scatter as can be observed in Figures 18 and 19. The scatter is too large to see any trends in the dark zone temperature; however, the NO concentration shows an increasing trend with increasing pressure—opposite from the JA-2 case.

4.4 Absorption - HMX2 Propellant. A nitramine composite propellant with a dark zone has also been investigated. The absorption data for this propellant was inferior to that of the other two propellants studied because of the much larger broadband absorption encountered. No OH data were obtained but one experimental run produced NO absorption data of sufficient quality for analysis. The temperatures and NO concentrations as a function of distance from the propellant surface are plotted in Figures 20 and 21. Video camera data indicate that the dark zone length is slightly less than 0.2 cm (see Figure 8); however, the measured NO concentration obtained from the absorption spectra has dropped considerably at this distance. It is conjectured that this immediate falloff of NO concentration is due to movements of the flame front which introduce path length regions that are NO depleted and, thus, the best estimate of the NO concentration in the dark zone of HMX2 is close to the propellant surface. In contrast, the temperature remains about constant (≈ 1,300 K) out to about 0.1 cm from the surface. Comparisons of HMX2, M9, and JA-2 propellant results obtained in this study, with available known literature data, are presented in the summary section.

5. SUMMARY

A comparison of dark zone temperatures (T_{dz}) and NO mole fractions (NO) obtained here with published data is shown in Table 2. The pressures (P) are not quite the same in all cases but this does not invalidate the comparison as these two variables are not strong functions of pressure within the dark zone. The calculated adiabatic flame temperatures (T_{ad}) and the heats of explosion (HOE) are also listed for each propellant. Heats of explosion are included since the dark zone temperatures have been ordered according to this parameter; see, for example, Beckstead (1989).

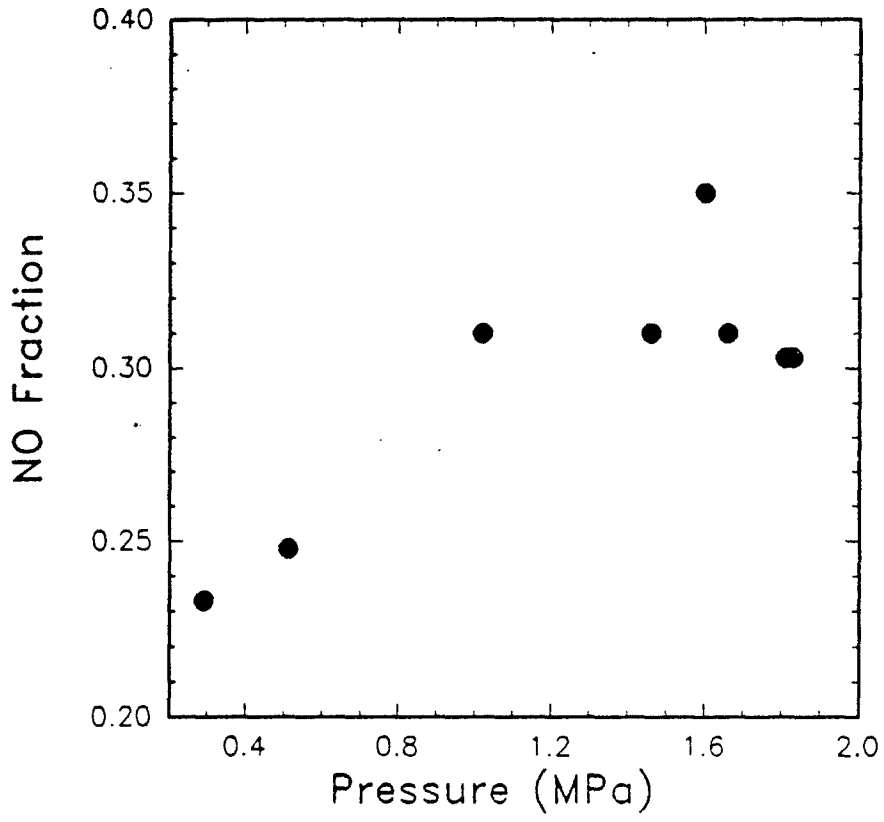

Figure 18. NO Concentration in the Dark Zone of M9 Propellant Obtained as a Function of Pressure.

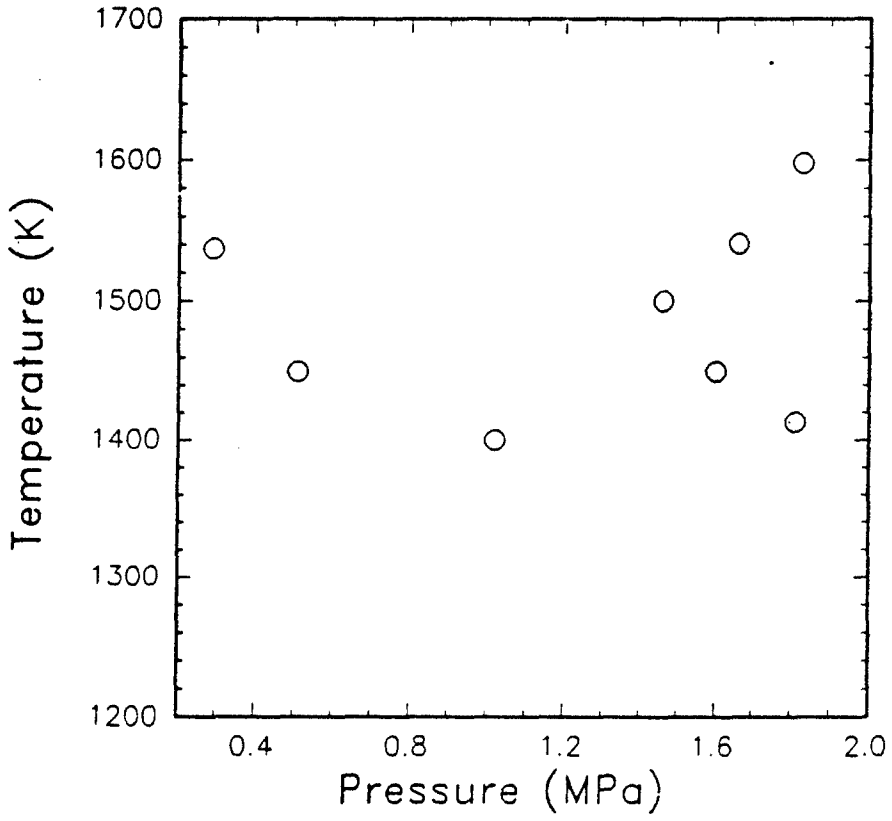

Figure 19. Dark Zone Temperature as a Function of Pressure for M9 Propellant.

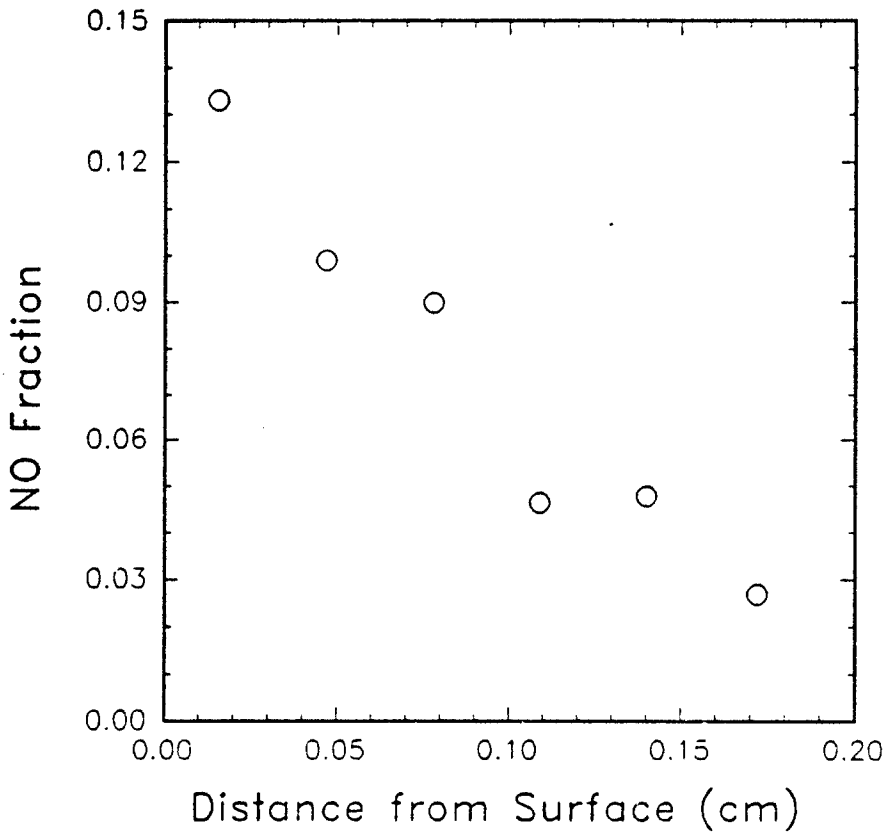

Figure 20. NO Concentration as a Function of Distance From the Propellant Surface for HMX2 Burning in 1.9 MPa Nitrogen.

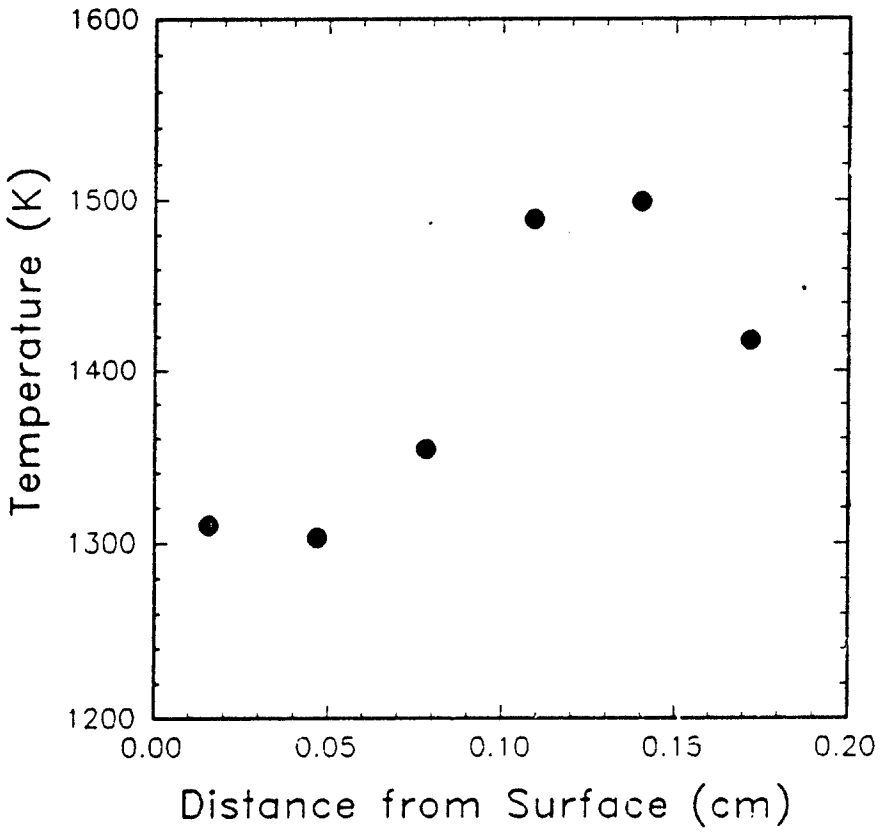

Figure 21. Temperature as a Function of Distance From the Propellant Surface for HMX2 Burning in 1.9 MPa Nitrogen.

Table 2. Comparison of Temperatures and NO Concentrations in the Dark Zone of Various Propellants

Propellant Type	JA-2	M9	Double Base[a]	Double Base[b]	HMX2	HMX - PE[c]
T_{ds}	1,450 K	1,500 K	1,600 K	1,500 K	1,310 K	1,300 K
P	1.6 MPa	1.6 MPa	1.6 MPa	0.9 MPa	1.9 MPa	2.0 MPa
NO	0.21	0.30	0.25†	0.21	0.13	0.17†
T_{ad}	2,791 K	3,019 K	3,094 K	2,897 K	2,045 K	1,912 K
HOE	1,120 Cal/g[d]	1,308 Cal/g[d]	1,320 Cal/g[e]	1,100 Cal/g[e]	780 Cal/g[f]	718 Cal/g[f]

† These mole fractions were recomputed assuming an H_2O mole fraction of 0.2.
[a] Heller and Gordon (1955).
[b] Lengelle et al. (1984).
[c] Kubota (1982).
[d] Measured quantity that is reported on the propellant description sheets.
[e] Given in the paper.
[f] Calculated from the empirical relationship to adiabatic flame temperature (Edwards 1988).

The data we obtain for M9 propellant is directly comparable with the double-base propellant literature data of Heller and Gordon since the ingredients and HOE's are almost identical. There is good agreement for the dark zone temperatures; only a 100 K difference which is within the experimental uncertainty of the experiments. The agreement for the NO concentration is excellent; however, the value recomputed from the data of Heller and Gordon assumes a 0.2 mole fraction H_2O present. Heller and Gordon suggest an H_2O value of 0.3 provides a best correlation for the elemental balance. The thermochemical equilibrium value of 0.27 mole fraction for H_2O should represent the upper limit for H_2O in the dark zone and, thus, we have chosen a value of 0.2. There is excellent agreement between our data for JA-2 propellant and the data of Lengelle et al (1984). Here the HOE's are about the same but the propellant ingredients are somewhat different (no DEGDN in the propellant of Lengelle et al. (1984). HMX2 propellant is similar to one of the propellants Kubota (1982) studied. The difference is in the binder; HMX2 has a polyester binder while the HMX-PE has a polyether binder. The measured dark zone temperatures are essentially the same and the NO concentration we obtain for HMX2 is about 25% greater than the HMX-PE where again a mole fraction of 0.2 was assumed in the computing of the NO mole fraction for HMX-PE.

Previous, intrusive type measurements in the dark zone of propellants have been verified and extended by the present data obtained by a nonintrusive technique—absorption spectroscopy. It remains to be seen

how well these data can be modelled and will be the subject of a future report. Sotter (1965) and Fifer et al. (1990) have been successful in modelling gas phase propellant combustion for a double-base propellant using the data of Heller and Gordon (1955); consequently, it should be straightforward to model the present data for M9 and JA-2. Perhaps the HMX2 data will be straightforward to model as well. Evidence to support this claim comes from the reasoning that the NO concentration in the dark zone is substantially less than for the double base propellant and, thus, not as much total energy is obtained in the conversion to N_2, thus leading to a lower final flame temperature which is indeed the case (T_{ad} = 2,045 K).

6. REFERENCES

Beckstead, M. W. "Modeling AN, AP, HMX and Double Base Monopropellants." 26th JANNAF Combustion Meeting, CPIA 529, vol. 4, p. 255, 1989.

Bizot, A., and M. W. Beckstead. "A Model for Double Base Propellant Combustion." 22nd Symposium (International) on Combustion, p. 1827, The Combustion Institute, 1988.

Edwards, T. "Solid Propellant Flame Spectroscopy." AFAL-TR-88-076, Edwards Air Force Base, CA, August 1988.

Fifer, R. A., A. J. Kotlar, M. S. Miller, and J. B. Morris. "Dark Zone Modeling for Delayed Ignition Studies." 27th JANNAF Combustion Meeting, November 1990.

Heller, C. A., and A. S. Gordon. "Structure of the Gas Phase Combustion Region of a Solid Double Base Propellant." Journal of Physical Chemistry, vol. 59, p. 773, 1955.

Huber, K. P., and G. Herzberg. Molecular Spectra and Molecular Structure. IV. Constants of Diatomic Molecules, Van Nostrand Reinhold Company, 1979.

Kubota, N. "Physiochemical Processes of HMX Propellant Combustion." 19th Symposium (International) on Combustion, p. 777, The Combustion Institute, 1982.

Lengelle, G., A. Bizot, J. Duterque, and J. F. Trubert. "Steady State Burning of Homogeneous Propellants." Fundamentals of Solid Propellant Combustion. Edited by K. Kuo and M. Summerfield. AIAA Progress in Astronautics and Aeronautics Series, vol. 90, 1984.

Lucht, R. P., R. C. Peterson, and N. M. Laurendeau. "Fundamentals of Absorption Spectroscopy for Selected Diatomic Radicals." PURDU-CL-78-06, 1978.

Sotter, J. G. "Chemical Kinetics of the Cordite Explosion Zone." 10th Symposium (International) on Combustion, p. 1405, The Combustion Institute, 1965.

Svehla, R. A., and B. J. McBride. "Fortran IV Computer Program for Calculation of Thermodynamic and Transport Properties of Complex Chemical Systems." NASA, TND-7056, 1973.

Vanderhoff, J. A. "Spectral Studies of Propellant Combustion: Experimental Details and Emission Results for M-30 Propellant." BRL-MR-3714, U.S. Army Ballistic Research Laboratory, Aberdeen Proving Ground, MD, 1988.

Vanderhoff, J. A. "Species Profiles in Solid Propellant Flames Using Absorption and Emission Spectroscopy." Combustion & Flame, vol. 84, p. 73, 1991.

Vanderhoff, J. A., and A. J. Kotlar. "Improving Spectral Fits of Absorption Data Taken with an Array Detector: Wavelength Linearization." BRL-MR-3866, U.S. Army Ballistic Research Laboratory, Aberdeen Proving Ground, MD, 1990a.

Vanderhoff, J. A., and A. J. Kotlar. "Simultaneous Determination of Temperature and OH Concentrations in a Solid Propellant Flame." 23rd Symposium (International) on Combustion, p. 1339, The Combustion Institute, 1990b.

Vanderhoff, J. A., A. J. Kotlar, and M. W. Teague. "Temperature and Concentrations of Combustion Radicals Obtained by Computer Fitting Absorption Spectra." 27th JANNAF Combustion Meeting, November 1990.

No. of Copies	Organization
2	Administrator Defense Technical Info Center ATTN: DTIC-DDA Cameron Station Alexandria, VA 22304-6145
1	Commander U.S. Army Materiel Command ATTN: AMCAM 5001 Eisenhower Ave. Alexandria, VA 22333-0001
1	Commander U.S. Army Laboratory Command ATTN: AMSLC-DL 2800 Powder Mill Rd. Adelphi, MD 20783-1145
2	Commander U.S. Army Armament Research, Development, and Engineering Center ATTN: SMCAR-IMI-I Picatinny Arsenal, NJ 07806-5000
2	Commander U.S. Army Armament Research, Development, and Engineering Center ATTN: SMCAR-TDC Picatinny Arsenal, NJ 07806-5000
1	Director Benet Weapons Laboratory U.S. Army Armament Research, Development, and Engineering Center ATTN: SMCAR-CCB-TL Watervliet, NY 12189-4050
(Unclass. only) 1	Commander U.S. Army Armament, Munitions, and Chemical Command ATTN: AMSMC-IMF-L Rock Island, IL 61299-5000
1	Director U.S. Army Aviation Research and Technology Activity ATTN: SAVRT-R (Library) M/S 219-3 Ames Research Center Moffett Field, CA 94035-1000
1	Commander U.S. Army Missile Command ATTN: AMSMI-RD-CS-R (DOC) Redstone Arsenal, AL 35898-5010

No. of Copies	Organization
1	Commander U.S. Army Tank-Automotive Command ATTN: ASQNC-TAC-DIT (Technical Information Center) Warren, MI 48397-5000
1	Director U.S. Army TRADOC Analysis Command ATTN: ATRC-WSR White Sands Missile Range, NM 88002-5502
1	Commandant U.S. Army Field Artillery School ATTN: ATSF-CSI Ft. Sill, OK 73503-5000
2	Commandant U.S. Army Infantry School ATTN: ATZB-SC, System Safety Fort Benning, GA 31903-5000
(Class. only) 1	Commandant U.S. Army Infantry School ATTN: ATSH-CD (Security Mgr.) Fort Benning, GA 31905-5660
(Unclass. only) 1	Commandant U.S. Army Infantry School ATTN: ATSH-CD-CSO-OR Fort Benning, GA 31905-5660
1	WL/MNME Eglin AFB, FL 32542-5000
	Aberdeen Proving Ground
2	Dir, USAMSAA ATTN: AMXSY-D AMXSY-MP, H. Cohen
1	Cdr, USATECOM ATTN: AMSTE-TC
3	Cdr, CRDEC, AMCCOM ATTN: SMCCR-RSP-A SMCCR-MU SMCCR-MSI
1	Dir, VLAMO ATTN: AMSLC-VL-D
10	Dir, USABRL ATTN: SLCBR-DD-T

No. of Copies | Organization

1 HQDA (SARD-TC, C.H. Church)
WASH DC 20310-0103

4 Commander
US Army Research Office
ATTN: R. Ghirardelli
D. Mann
R. Singleton
R. Shaw
P.O. Box 12211
Research Triangle Park, NC
27709-2211

2 Commander
US Army Armament Research,
Development, and Engineering Center
ATTN: SMCAR-AEE-B, D.S. Downs
SMCAR-AEE, J.A. Lannon
Picatinny Arsenal, NJ 07806-5000

1 Commander
US Army Armament Research,
Development, and Engineering Center
ATTN: SMCAR-AEE-BR, L. Harris
Picatinny Arsenal, NJ 07806-5000

2 Commander
US Army Missile Command
ATTN: AMSMI-RD-PR-E, A.R. Maykut
AMSMI-RD-PR-P, R. Betts
Redstone Arsenal, AL 35898-5249

1 Office of Naval Research
Department of the Navy
ATTN: R.S. Miller, Code 432
800 N. Quincy Street
Arlington, VA 22217

1 Commander
Naval Air Systems Command
ATTN: J. Ramnarace, AIR-54111C
Washington, DC 20360

1 Commander
Naval Surface Warfare Center
ATTN: J.L. East, Jr., G-23
Dahlgren, VA 22448-5000

No. of Copies | Organization

2 Commander
Naval Surface Warfare Center
ATTN: R. Bernecker, R-13
G.B. Wilmot, R-16
Silver Spring, MD 20903-5000

5 Commander
Naval Research Laboratory
ATTN: M.C. Lin
J. McDonald
E. Oran
J. Shnur
R.J. Doyle, Code 6110
Washington, DC 20375

1 Commanding Officer
Naval Underwater Systems
Center Weapons Dept.
ATTN: R.S. Lazar/Code 36301
Newport, RI 02840

2 Commander
Naval Weapons Center
ATTN: T. Boggs, Code 388
T. Parr, Code 3895
China Lake, CA 93555-6001

1 Superintendent
Naval Postgraduate School
Dept. of Aeronautics
ATTN: D.W. Netzer
Monterey, CA 93940

3 AL/LSCF
ATTN: R. Corley
R. Geisler
J. Levine
Edwards AFB, CA 93523-5000

1 AFOSR
ATTN: J.M. Tishkoff
Bolling Air Force Base
Washington, DC 20332

1 OSD/SDIO/IST
ATTN: L. Caveny
Pentagon
Washington, DC 20301-7100

No. of Copies	Organization
1	Commandant USAFAS ATTN: ATSF-TSM-CN Fort Sill, OK 73503-5600
1	F.J. Seiler ATTN: S.A. Shackleford USAF Academy, CO 80840-6528
1	University of Dayton Research Institute ATTN: D. Campbell AL/PAP Edwards AFB, CA 93523
1	NASA Langley Research Center Langley Station ATTN: G.B. Northam/MS 168 Hampton, VA 23365
4	National Bureau of Standards ATTN: J. Hastie M. Jacox T. Kashiwagi H. Semerjian US Department of Commerce Washington, DC 20234
1	Aerojet Solid Propulsion Co. ATTN: P. Micheli Sacramento, GA 95813
1	Applied Combustion Technology, Inc. ATTN: A.M. Varney P.O. Box 607885 Orlando, FL 32860
2	Applied Mechanics Reviews The American Society of Mechanical Engineers ATTN: R.E. White A.B. Wenzel 345 E. 47th Street New York, NY 10017
1	Atlantic Research Corp. ATTN: R.H.W. Waesche 7511 Wellington Road Gainesville, VA 22065

No. of Copies	Organization
1	AVCO Everett Research Laboratory Division ATTN: D. Stickler 2385 Revere Beach Parkway Everett, MA 02149
1	Battelle ATTN: TACTEC Library, J. Huggins 505 King Avenue Columbus, OH 43201-2693
1	Cohen Professional Services ATTN: N.S. Cohen 141 Channing Street Redlands, CA 92373
1	Exxon Research & Eng. Co. ATTN: A. Dean Route 22E Annandale, NJ 08801
1	General Applied Science Laboratories, Inc. 77 Raynor Avenue Ronkonkama, NY 11779-6649
1	General Electric Ordnance Systems ATTN: J. Mandzy 100 Plastics Avenue Pittsfield, MA 01203
1	General Motors Rsch Labs Physical Chemistry Department ATTN: T. Sloane Warren, MI 48090-9055
2	Hercules, Inc. Allegheny Ballistics Lab. ATTN: W.B. Walkup E.A. Yount P.O. Box 210 Rocket Center, WV 26726
1	Alliant Techsystems, Inc. Marine Systems Group ATTN: D.E. Broden/ MS MN50-2000 600 2nd Street NE Hopkins, MN 55343

No. of Copies | Organization

1 Alliant Techsystems, Inc.
ATTN: R.E. Tompkins
MN38-3300
5700 Smetana Drive
Minnetonka, MN 55343

1 IBM Corporation
ATTN: A.C. Tam
Research Division
5600 Cottle Road
San Jose, CA 95193

1 IIT Research Institute
ATTN: R.F. Remaly
10 West 35th Street
Chicago, IL 60616

2 Director
Lawrence Livermore
National Laboratory
ATTN: C. Westbrook
M. Costantino
P.O. Box 808
Livermore, CA 94550

1 Lockheed Missiles & Space Co.
ATTN: George Lo
3251 Hanover Street
Dept. 52-35/B204/2
Palo Alto, CA 94304

1 Director
Los Alamos National Lab
ATTN: B. Nichols, T7, MS-B284
P.O. Box 1663
Los Alamos, NM 87545

1 National Science Foundation
ATTN: A.B. Harvey
Washington, DC 20550

1 Olin Ordnance
ATTN: V. McDonald, Library
P.O. Box 222
St. Marks, FL 32355-0222

1 Paul Gough Associates, Inc.
ATTN: P.S. Gough
1048 South Street
Portsmouth, NH 03801-5423

No. of Copies | Organization

2 Princeton Combustion
Research Laboratories, Inc.
ATTN: M. Summerfield
N.A. Messina
475 US Highway One
Monmouth Junction, NJ 08852

1 Hughes Aircraft Company
ATTN: T.E. Ward
8433 Fallbrook Avenue
Canoga Park, CA 91303

1 Rockwell International Corp.
Rocketdyne Division
ATTN: J.E. Flanagan/HB02
6633 Canoga Avenue
Canoga Park, CA 91304

4 Director
Sandia National Laboratories
Division 8354
ATTN: R. Cattolica
S. Johnston
P. Mattern
D. Stephenson
Livermore, CA 94550

1 Science Applications, Inc.
ATTN: R.B. Edelman
23146 Cumorah Crest
Woodland Hills, CA 91364

3 SRI International
ATTN: G. Smith
D. Crosley
D. Golden
333 Ravenswood Avenue
Menlo Park, CA 94025

1 Stevens Institute of Tech.
Davidson Laboratory
ATTN: R. McAlevy, III
Hoboken, NJ 07030

1 Sverdrup Technology, Inc.
LERC Group
ATTN: R.J. Locke, MS SVR-2
2001 Aerospace Parkway
Brook Park, OH 44142

No. of Copies | Organization

1 Sverdrup Technology, Inc.
ATTN: J. Deur
2001 Aerospace Parkway
Brook Park, OH 44142

1 Thiokol Corporation
Elkton Division
ATTN: S.F. Palopoli
P.O. Box 241
Elkton, MD 21921

3 Thiokol Corporation
Wasatch Division
ATTN: S.J. Bennett
P.O. Box 524
Brigham City, UT 84302

1 United Technologies Research Center
ATTN: A.C. Eckbreth
East Hartford, CT 06108

3 United Technologies Corp.
Chemical Systems Division
ATTN: R.S. Brown
T.D. Myers (2 copies)
P.O. Box 49028
San Jose, CA 95161-9028

1 Universal Propulsion Company
ATTN: H.J. McSpadden
Black Canyon Stage 1
Box 1140
Phoenix, AZ 85029

1 Veritay Technology, Inc.
ATTN: E.B. Fisher
4845 Millersport Highway
P.O. Box 305
East Amherst, NY 14051-0305

1 Brigham Young University
Dept. of Chemical Engineering
ATTN: M.W. Beckstead
Provo, UT 84058

1 California Institute of Tech.
Jet Propulsion Laboratory
ATTN: L. Strand/MS 512/102
4800 Oak Grove Drive
Pasadena, CA 91109

No. of Copies | Organization

1 California Institute of Technology
ATTN: F.E.C. Culick/MC 301-46
204 Karman Lab.
Pasadena, CA 91125

1 University of California
Los Alamos Scientific Lab.
P.O. Box 1663, Mail Stop B216
Los Alamos, NM 87545

1 University of California, Berkeley
Chemistry Deparment
ATTN: C. Bradley Moore
211 Lewis Hall
Berkeley, CA 94720

1 University of California, San Diego
ATTN: F.A. Williams
AMES, B010
La Jolla, CA 92093

2 University of California, Santa Barbara
Quantum Institute
ATTN: K. Schofield
M. Steinberg
Santa Barbara, CA 93106

1 University of Colorado at Boulder
Engineering Center
ATTN: J. Daily
Campus Box 427
Boulder, CO 80309-0427

2 University of Southern California
Dept. of Chemistry
ATTN: S. Benson
C. Wittig
Los Angeles, CA 90007

1 Cornell University
Department of Chemistry
ATTN: T.A. Cool
Baker Laboratory
Ithaca, NY 14853

No. of Copies | Organization

1 University of Delaware
ATTN: T. Brill
Chemistry Department
Newark, DE 19711

1 University of Florida
Dept. of Chemistry
ATTN: J. Winefordner
Gainesville, FL 32611

3 Georgia Institute of Technology
School of Aerospace Engineering
ATTN: E. Price
W.C. Strahle
B.T. Zinn
Atlanta, GA 30332

1 University of Illinois
Dept. of Mech. Eng.
ATTN: H. Krier
144MEB, 1206 W. Green St.
Urbana, IL 61801

1 Johns Hopkins University/APL
Chemical Propulsion
Information Agency
ATTN: T.W. Christian
Johns Hopkins Road
Laurel, MD 20707

1 University of Michigan
Gas Dynamics Lab
Aerospace Engineering Bldg.
ATTN: G.M. Faeth
Ann Arbor, MI 48109-2140

1 University of Minnesota
Dept. of Mechanical
Engineering
ATTN: E. Fletcher
Minneapolis, MN 55455

3 Pennsylvania State University
Applied Research Laboratory
ATTN: K.K. Kuo
H. Palmer
M. Micci
University Park, PA 16802

No. of Copies | Organization

1 Pennsylvania State University
Dept. of Mechanical Engineering
ATTN: V. Yang
University Park, PA 16802

1 Polytechnic Institute of NY
Graduate Center
ATTN: S. Lederman
Route 110
Farmingdale, NY 11735

2 Princeton University
Forrestal Campus Library
ATTN: K. Brezinsky
I. Glassman
P.O. Box 710
Princeton, NJ 08540

1 Purdue University
School of Aeronautics
and Astronautics
ATTN: J.R. Osborn
Grissom Hall
West Lafayette, IN 47906

1 Purdue University
Department of Chemistry
ATTN: E. Grant
West Lafayette, IN 47906

2 Purdue University
School of Mechanical
Engineering
ATTN: N.M. Laurendeau
S.N.B. Murthy
TSPC Chaffee Hall
West Lafayette, IN 47906

1 Rensselaer Polytechnic Inst.
Dept. of Chemical Engineering
ATTN: A. Fontijn
Troy, NY 12181

1 Stanford University
Dept. of Mechanical
Engineering
ATTN: R. Hanson
Stanford, CA 94305

No. of Copies	Organization
1	University of Texas Dept. of Chemistry ATTN: W. Gardiner Austin, TX 78712
1	University of Utah Dept. of Chemical Engineering ATTN: G. Flandro Salt Lake City, UT 84112
1	Virginia Polytechnic Institute and State University ATTN: J.A. Schetz Blacksburg, VA 24061
1	Freedman Associates ATTN: E. Freedman 2411 Diana Road Baltimore, MD 21209-1525

INTENTIONALLY LEFT BLANK.

USER EVALUATION SHEET/CHANGE OF ADDRESS

This laboratory undertakes a continuing effort to improve the quality of the reports it publishes. Your comments/answers below will aid us in our efforts.

1. Does this report satisfy a need? (Comment on purpose, related project, or other area of interest for which the report will be used.) _____

2. How, specifically, is the report being used? (Information source, design data, procedure, source of ideas, etc.) _____

3. Has the information in this report led to any quantitative savings as far as man-hours or dollars saved, operating costs avoided, or efficiencies achieved, etc? If so, please elaborate. _____

4. General Comments. What do you think should be changed to improve future reports? (Indicate changes to organization, technical content, format, etc.) _____

BRL Report Number BRL-TR-3334 Division Symbol _____

Check here if desire to be removed from distribution list. ____

Check here for address change. ____

Current address: Organization _____
Address _____
_____

DEPARTMENT OF THE ARMY
Director
U.S. Army Ballistic Research Laboratory
ATTN: SLCBR-DD-T
Aberdeen Proving Ground, MD 21005-5066

OFFICIAL BUSINESS

BUSINESS REPLY MAIL
FIRST CLASS PERMIT No 0001, APG, MD

Postage will be paid by addressee.

Director
U.S. Army Ballistic Research Laboratory
ATTN: SLCBR-DD-T
Aberdeen Proving Ground, MD 21005-5066

NO POSTAGE
NECESSARY
IF MAILED
IN THE
UNITED STATES